Desalination and Water Treatment
www.deswater.com
doi: 10.5004/dwt.2021.26963

219 (2021) 413–422
April

Comparing watershed management strategies at different spatial scales under future climate scenarios using SWAT

Heewon Jeong[a,†], Bumjo Kim[a,†], Joon Ha Kim[a], Sung Ju Yi[b], Jong Doo Kim[c], Seo Jin Ki[d,*]

[a]*School of Earth Sciences and Environmental Engineering (SESE), Gwangju Institute of Science and Technology (GIST), Gwangju 61005, Republic of Korea, emails: gua01114@gist.ac.kr (H. Jeong), bumjo@gist.ac.kr (B. Kim), joonkim@gist.ac.kr (J.H. Kim)*
[b]*Department of Civil, Environmental and Biomedical Engineering, Graduate School, Sangmyung University, Cheonan, Republic of Korea, email: ysjibo@keco.or.kr*
[c]*Civil Engineering and Plant Business, KUMHO E&C, Republic of Korea, email: jdkim1@kumhoenc.com*
[d]*Department of Environmental Engineering, Gyeongnam National University of Science and Technology, Jinju 52725, Republic of Korea, Tel. +82-55-751-3341; email: seojinki@gntech.ac.kr*

Received 13 August 2020; Accepted 4 December 2020

ABSTRACT

It is essential that water resource management plans require explicit links across different spatial scales in a single watershed. This study aimed to identify existing gaps between sub-basin and watershed management strategies using a watershed simulation model soil and water assessment tool (SWAT). The SWAT was calibrated and validated at the upper and middle regions of the Yeongsan River in Korea using past weather inputs from 2012 to 2014. The simulation outputs from 2014 used as a reference were compared to those with future weather scenarios in 2032 produced from a regional climate model (RCM) such as RCM 2.6, 4.5, 6.0, and 8.5. We found that the calibration and validation results agreed well with the observed data, yielding Nash–Sutcliffe efficiency values more than 0.72 for daily streamflow as well as for monthly sediment and total phosphorus (TP) loads at the final watershed outlet. However, all projected weather data led to a significant difference in streamflow only at the sub-basin level, while all three variables at the watershed level varied significantly from scenario to scenario. These imply that water resource management plans determined at the watershed scale may not be suitable for those at the sub-basin scale, calling for a more refined search that harmonizes both management decisions.

Keywords: SWAT; Regional Climate Model; Future weather scenarios; Climate change; Watershed management plans

1. Introduction

Watershed management provides a framework for restoring impaired water resources as well as promoting the sustainable use of watershed resources and functions [1,2]. Watershed management plans were developed and adjusted through iterative process so that continuous improvements in water quality and quantity should be attained [1,2]. Monitoring data compiled from various watershed management programs helped not only characterize pollution hotspots and priority pollutants, but also assess the effectiveness of pollution reduction strategies during the repeated management cycles. Watershed or water quality models also assisted in the watershed planning process by estimating pollutant load reductions in response to a series of management options and anticipated changes of environmental conditions [3]. Those models were particularly valuable in capturing water flow and solute transport which varied widely across time and space, and thus, were proposed for various simulation

* Corresponding author.

† These authors have contributed equally to this work.

studies for both ungauged and gauged watersheds [4]. Using either statistical analysis or mathematical models, it is important that management plans for smaller watersheds support the strengthening of those activities for large basins.

The soil and water assessment tool (SWAT) is one of simulation tools extensively adopted in prioritizing available management options in a given watershed, including total maximum daily load (TMDL) development [5]. For example, Aghakhani et al. [5] examined the relationship between land use activities and surface runoff using the SWAT, and found that a combination of land management practices resulted in reduction of surface runoff by 6%–22.3%. In addition, adaptation strategies for future weather changes were studied with several SWAT applications [6–8]. Specifically, Ahmadi et al. [6] found that ecological health and drinking water supplies were vulnerable to the projected increase in pollutant fluxes. The study of Carvalho-Santos et al. [7] revealed that the construction of a new reservoir only addressed the shortage of water supply in the target watershed under current climate conditions rather than under future climate conditions. Babur et al. [8] showed that (two) future climate projections led to the increasing number of days with high streamflow, but a decrease in median streamflow. There were some studies that addressed the isolated and combined effects of those influencing factors (e.g., climate and land use changes) on streamflow and pollutant fluxes using SWAT [9,10]. In other studies, the SWAT was often employed to evaluate the effectiveness of best management practices (BMP) strategies against changing environmental conditions such as land use and climate alteration [11–13]. Some earlier studies also provided evidence for the validity and reliability of the SWAT model in the TMDL analyses [3,14].

This study aimed to identify the consistency of management strategies between small and large drainage basins using the SWAT model, as compared to previous studies. This is because even though integrated watershed management emphasizes proper coordination of management plans at different spatial scales, these are generally ignored by many modeling studies. Using the SWAT model, specific objectives were (1) to determine the optimal parameter set in the selected watershed, (2) to produce baseline simulation results for three variables of interest, and (3) to compare new prediction results with future weather inputs to those obtained during the baseline period. We hope that the proposed mythology will facilitate integration efforts and implementation efficiency of watershed management plans at both various spatial and temporal scales.

2. Materials and methods

2.1. Study area

The upper and middle regions of Yeongsan (YS) River watershed were selected as the target study area for simulation of water quantity and quality (Fig. 1). The YS River watershed, which covers an area of 3,371 km^2, is located in the south western part of Korean Peninsula and runs from Damyang (upstream) through Gwangju and Naju (midstream) eventually to the Yellow Sea in Mokpo (downstream) [15]. Out of the entire watershed area, the selected watershed has a drainage area of 2,938 km^2. The watershed experienced chronic pollutant inputs from intensive agricultural activities. In fact, land use over the whole watershed is dominated by 50% of forest, 29% of cropland, 12% of urban area, and 9% of water [16]. According to historical rainfall records for the period 1966–2014, the watershed received an average of 1,301 mm of precipitation annually [17]. To prepare the weather input files for simulation, the daily rainfall data was obtained at nine stations (i.e., eight precipitation gauges plus one regular weather station) from 2012 to 2014. In contrast, the air temperature, wind speed, and relative humidity were also collected from the regular weather station (Fig. 1). The compiled data represented the current local weather conditions, and served as a baseline in subsequent simulations with future weather scenarios (section 2.2 – compilation of future weather inputs). The Sapo monitoring station, which was routinely monitored by the Ministry of Land, Infrastructure, and Transport of Korea, was selected as the final outlet of the selected watershed (Fig. 1).

2.2. Compilation of future weather inputs

The future climate scenarios for 2014–2032 simulated with the regional climate model (RCM) HadGEM3-RA were compiled from the climate information portal of Korea [18]. The standard HadGEM3-RA product has 12.5 km spatial resolution, and contains four projection scenarios (RCM 2.6, 4.5, 6.0, and 8.5) depending on the radiative forcing levels from lowest to highest. As described in the current weather inputs, air temperature, precipitation, wind speed, and relative humidity were provided as inputs to the simulation model. Note that the RCM provides a single value (for individual parameters) covering an area of approximately 160 km^2. Each value is thus assigned to one or multiple outlets of individual sub-basins, which make up the selected watershed (section 2.3 – SWAT model set up) within an evenly spaced grid. Before introducing the future weather scenarios into the simulation model, a bias correction for the RCM data was made to match the observation data at the nine precipitation stations in the selected watershed [19,20]. The basic assumption behind the bias correction method is that the correction algorithm and its parameterization determined at the current weather conditions are identically maintained in the future weather scenarios. A dual approach combining local intensity scaling and power transformation enables correction of the mean, variance, and frequency of the precipitation simultaneously. The remaining parameters, including temperature, wind speed, and humidity were adjusted by a linear scaling correction. More detailed information on the bias correction for individual parameters is available in Appendix A [21].

2.3. SWAT model set up

The selected watershed was delineated based on both the digital elevation model (DEM) and the stream network generated from the built-in stream definition function in the SWAT. This resulted in 25 sub-basins in the selected watershed after the automatic delineation process. Individual

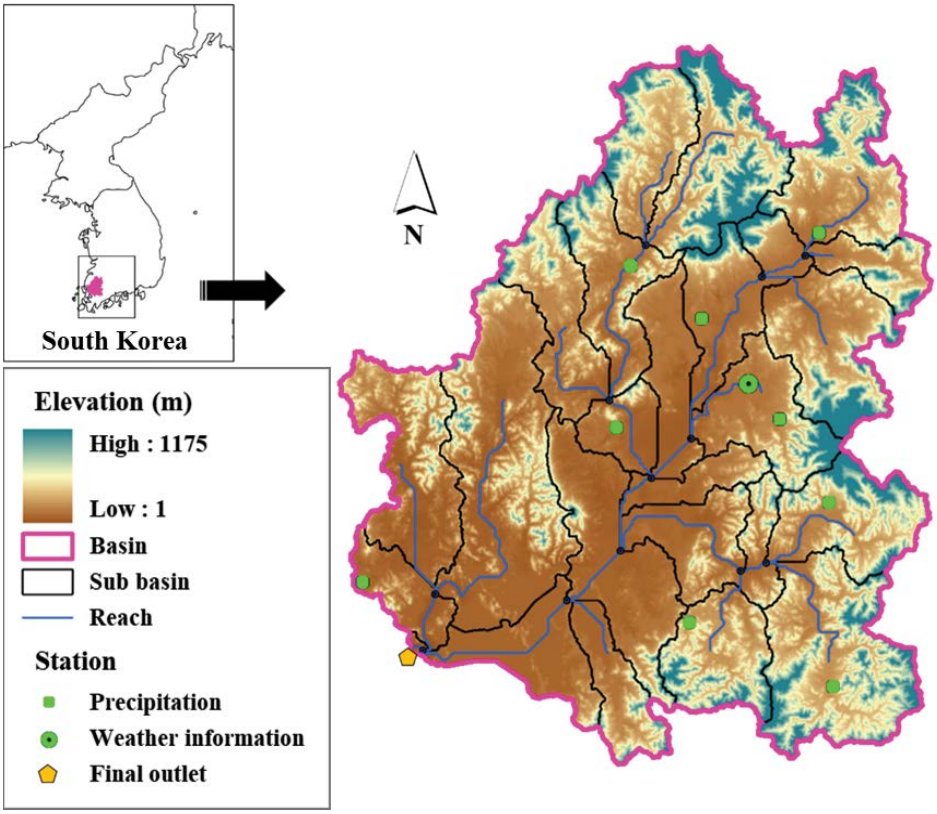

Fig. 1. Geographical location of the study area: the upper and middle regions of the Yeongsan River watershed.

sub-basins were then further segmented into one or multiple hydraulic response units (HRU) by adjusting the ratio of land use, soil class, and slope. A 5% threshold value was adopted for classifications of land use, soil, and slope when further partitioning sub-basins to HRU. Note that a single slope option for each HRU is used during the analysis because the YS watershed consists of fairly flat land. This, in turn, appears to reduce complexity and execution time related to hydrologic and water quality processes in the model. The simulation period of the SWAT model using the current weather inputs was set to 3 years (2012–2014), but specifically calibrated for the years 2012–2013, and validated for the period of 2014. The SWAT simulation was intended to produce outputs for daily streamflow as well as monthly sediment and total phosphorus (TP) loads.

2.4. Sensitivity analysis

Sensitivity analysis prioritizes the key parameters that are influential to the model output [22,23]. Sensitivity assesses the response of an output variable to a change in parameters. Out of various sensitivity analysis techniques, we specifically adopted the Latin hypercube one factor at a time (LH-OAT) method which was widely applied for global sensitivity analysis in surface and subsurface models. The LH-OAT combined the OAT design with Latin hypercube (LH) sampling by accepting the LH samples as initial points for an OAT design. The LH sampling method was carried out based on the Monte Carlo simulations, but employed a successively hierarchical sampling approach for the efficient estimation of output statistics [24]. A detailed procedure for the LH sampling and OAT design is described in van Griensven et al. [25] and Morris [26]. The change in model output can be attributed to the change of input parameter(s) by means of the partial effect $S_{i,j}$, which is given by:

$$S_{i,j} = \left[\frac{\mathrm{SSE}\left(e_1,\ldots,e_i\times\left(1+f\right),\ldots,e_p\right) - \mathrm{SSE}\left(e_1,\ldots,e_i,\ldots,e_p\right)}{f} \right] \quad (1)$$

where $S_{i,j}$ represents a partial effect for parameter e_i around an LH point j. f is the fraction by which the parameter e_i is changed (a predefined constant). SSE refers to the sum of squared errors. Note that considering p parameters, $(p + 1)$ model runs should be executed during the sensitivity analysis. The effects of individual parameters are quantified by averaging the partial effects of each loop for all LH points. Then, their priority is determined based on the relative contribution to the model output. Note that we specify the acceptable parameter variation range for the sensitivity analysis according to the SWAT input/output document [27].

2.5. Performance assessment and data analysis

As described earlier, the SWAT model was calibrated and validated for daily streamflow as well as monthly

pollutant loads with the observed data at the main outlet in the selected watershed. The calibration for streamflow as well as sediment and TP loads was done only using a set of parameters recommended from the sensitivity analysis. The performance of the SWAT model was assessed in terms of the coefficient of determination (R^2), the Nash–Sutcliffe efficiency (NSE), and the root mean square error (RMSE). The differences between baseline simulation (under the current weather input in 2014) and new predictions (under the future weather input in 2032) were quantified in terms of the average annual rate of change for three target variables. The nonparametric Kruskal–Wallis test was specifically adopted to assess statistical significance in these outputs among the sub-basins in reach RCM scenario as well as among RCM scenarios at the watershed level.

3. Results and discussions

3.1. Sensitivity analysis results

Table 1 provides a list of calibration parameters for three target variables (i.e., streamflow, sediment, and TP) and their optimized values in the SWAT model [28]. Note that the selected parameters are recommended from the sensitivity analysis, and are then ranked in descending order of importance for each variable. It was shown from the table that seven parameters out of a total of 27 were found to have a significant influence on the output streamflow. Specifically, the input parameter CN2, which indicated the initial runoff curve number for moisture condition II, had the highest sensitivity. The parameters ALPHA_BF and CH_K2, which were related to the processes of baseflow and channel routing, were ranked second and third, respectively. In contrast, four parameters played an important role in calculating the amount of sediment in the SWAT model. The parameter SPCON, which was involved in the channel sediment routing process, was ranked first. It was followed by PRF and CH_COV which were used as the adjustment factor for sediment routing and channel cover factor, respectively. Finally, seven parameters with high sensitivity were involved in the computation of TP. The highest ranks were assigned to EROGRP, BIOMIX, and PSP. The three parameters are associated with the phosphorous enrichment ratio for sediment loading, biological mixing efficiency, and phosphorous availability index, respectively. Note that all of the calibrated parameter sets are frequently reported in numerous sensitivity analyses in the SWAT literature as well as are within the range of allowable values in the user manual.

3.2. Calibration and validation results

The SWAT model was successfully calibrated and validated for the selected watershed. Fig. 2 compares the predicted and observed values for streamflow as well as sediment and TP loads at the watershed outlet during the calibration and validation periods. The predictive performance of the model for streamflow (Fig. 2a) as well as sediment and TP loads (Figs. 2b and c) is assessed in terms of NSE, R^2, and RMSE separately for each period. As shown in the Fig. 2, the SWAT model showed better performance during calibration than during validation with respect to NSE (for sediment and TP loads). A slight performance improvement was observed during the validation period in terms of R^2 rather

Table 1
Optimal set of input parameters determined during the SWAT calibration

Variables	Processes	Input parameters	Acceptable ranges[a]	Calibrated values
Streamflow	Hydrological cycle (for surface runoff)	CN2	−25.00–25.00	–0.95
	Hydrological cycle (for groundwater)	ALPHA_BF	0.00–1.00	0.99
	Channel processes (for channel water routing)	CH_K2	0.00–150.00	2.24
	Hydrological cycle (for surface runoff)	SURLAG	0.00–10.00	8.34
	Channel processes (for channel water routing)	CH_N2	0.00–1.00	0.45
	Hydrological cycle (for groundwater)	GWQMN	−1,000.00–1,000.00	586.05
	Hydrological cycle (Evapotranspiration)	ESCO	0.00–1.00	0.64
Sediment	Channel processes (for channel sediment routing)	SPCON	0.0001–0.01	0.001
	Channel processes (for channel sediment routing)	PRF	0–2.0	0.50
	Channel processes (for channel sediment routing)	CH_COV	−0.001–1.00	0
	Sediment (for sediment erosion)	USLE_P	0.10–0.90	0.10
Total phosphorus (TP)	Nutrients (for phosphorous cycle)	ERORGP	0.00–5.00	0.55
	Nutrients (for phosphorous cycle)	BIOMIX	0.0–1.00	0.10
	Nutrients (for phosphorous cycle)	PSP	0.20–0.60	0.60
	Channel processes (for channel nutrient routing)	BC4	0.10–0.70	0.10
	Nutrients (for phosphorous cycle)	GWSOLP	0.00–1.00	0
	Channel processes (for channel water quality indices)	RHOQ	0.05–0.50	0.05
	Channel processes (for channel water quality indices)	MUMAX	1.00–3.00	1.00

[a]Note that the acceptable range of input parameters were determined according to the SWAT input/output document [28].

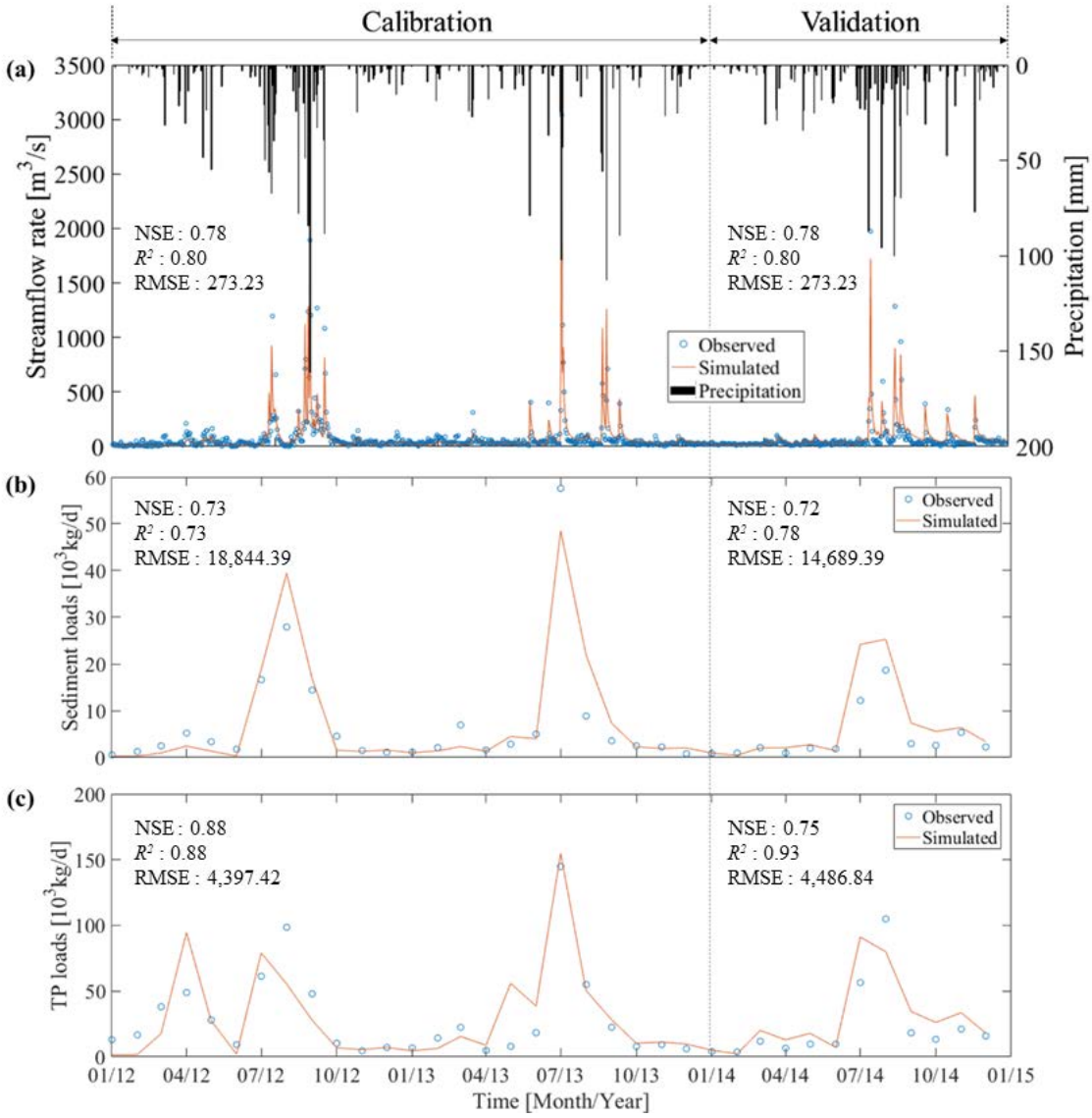

Fig. 2. Time series plots of observed and predicted variables in the final watershed outlet during the calibration and validation periods: (a) streamflow, (b) sediment loads, and (c) TP loads. Note that the black bar in (a) indicates the average daily precipitation estimated from a series of weather stations in the target watershed (Fig. 1).

than RMSE (for sediment and TP loads). However, in the case of streamflow, there were no significant differences in the overall performance of the model during both periods. Note that the values of NSE and R^2 approaching one indicates a perfect match between the predicted and observed ones, whereas RMSE is close to zero in such a case. A time series graph also revealed that the predicted results were generally in good agreement with the observed data during both periods, except for the monsoon season which led to heavy rainfall every year. Accordingly, we used the successful validation results in 2014 as a baseline for comparison with those obtained from future climate projections in 2032. The SWAT outputs calculated for streamflow, sediment loads, and TP loads at the sub-basin level in water year 2014 are visualized in Figs. 3a–c, respectively. Fig. 3 shows that streamflow and two pollutant loads generally become larger in downstream areas than upstream areas, albeit not increasing monotonically from upstream to downstream. These implied why hydrology and pollutant transport processes should be carefully assessed at the sub-basin scale under different environmental conditions such as new weather scenarios.

3.3. Impact of climate change on watershed processes

3.3.1. Impact on streamflow

Fig. 4 illustrates future changes in streamflow at 25 individual sub-basins predicted under different RCM scenarios, 2.6, 4.5, 6.0, and 8.5. The color bar indicates the percent change in the mean annual streamflow between baseline condition (in 2014) and a series of new predictions (in 2032). It was found that streamflow increased dramatically

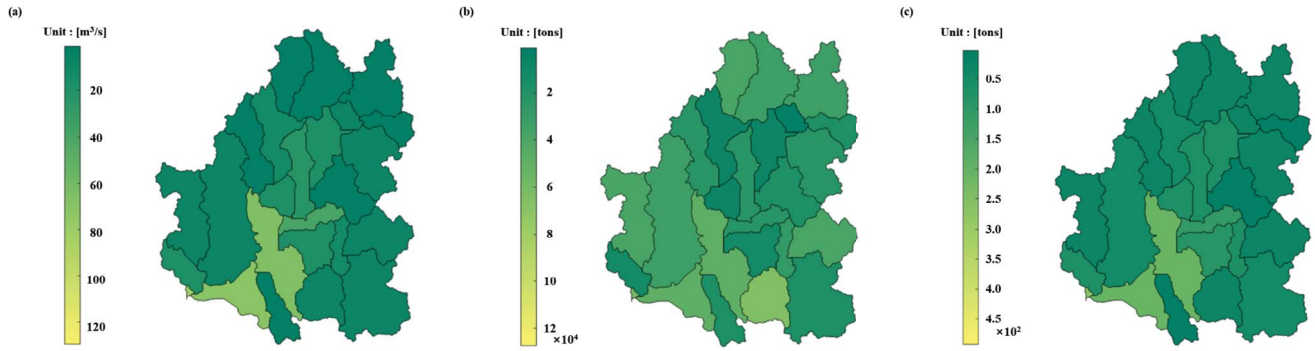

Fig. 3. Baseline evaluation for (a) streamflow, (b) sediment loads, and (c) TP loads at 25 sub-basins for water year 2014 using SWAT.

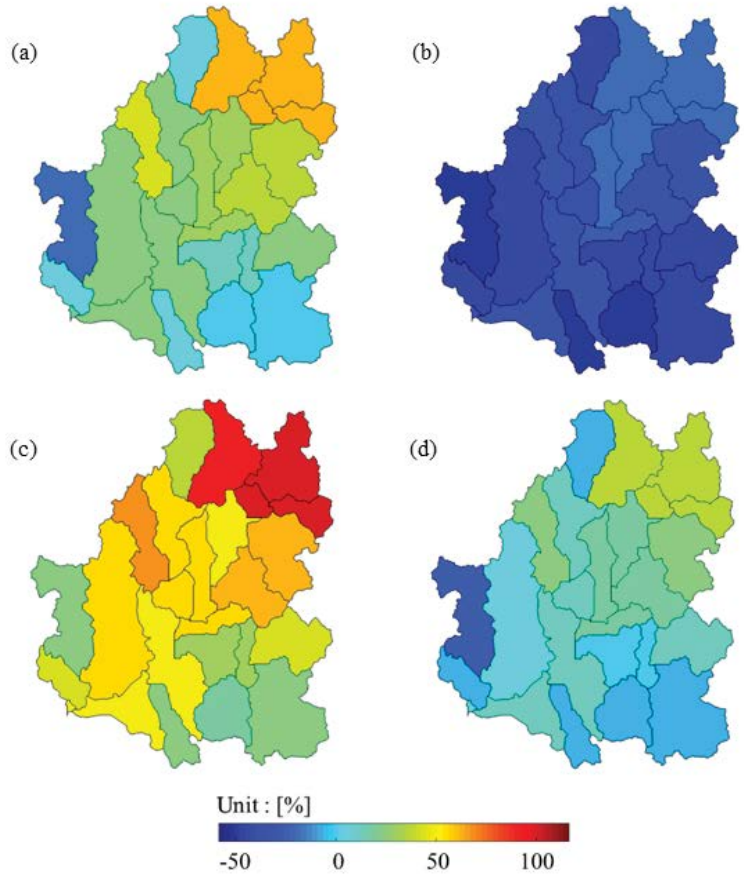

Fig. 4. Percent changes (%) in the predicted streamflow at the sub-basin scale under different future weather inputs in 2032: (a) RCM 2.6, (b) RCM 4.5, (c) RCM 6.0, and (d) RCM 8.5.

under RCM 6.0 scenario (Fig. 4c), whereas RCM 4.5 projection rather resulted in a considerable reduction of streamflow in all sub-basins (Fig. 4b). In fact, streamflow at a few upstream sub-basins in RCM 6.0 was more than double that of water year 2014. In the case of RCM 4.5, streamflow was decreased by half at maximum. Similar to the prediction result with RCM 6.0, both RCM 2.6 and 8.5 scenarios increased the output streamflow, although RCM 2.6 was more influential than RCM 8.5 (Figs. 4a and d). These results implied that streamflow in the target watershed was highly sensitive to (changing) weather conditions, but did not always increase linearly according to the radiative forcing levels.

3.3.2. *Impact on sediment loads*

The influence of RCM projections on the sediment loads at individual sub-basins is displayed in Fig. 5. In Fig. 5, the range of the color bar is set to vary approximately from –70% to 430% in terms of the percent change.

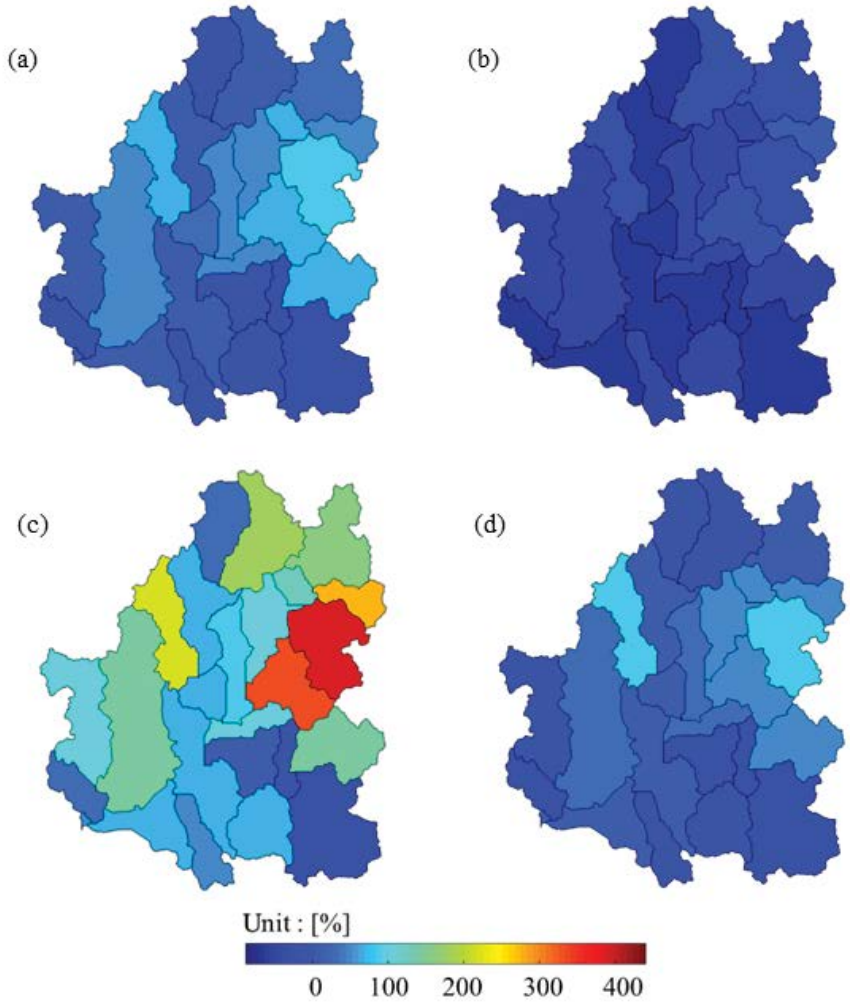

Fig. 5. Percent changes (%) in the predicted sediment loads at the sub-basin scale under different future weather inputs in 2032: (a) RCM 2.6, (b) RCM 4.5, (c) RCM 6.0, and (d) RCM 8.5.

As observed in streamflow, the mean annual sediment loads increased, to a large extent, throughout the sub-basins for RCM 6.0 scenario (Fig. 5c), when comparing other prediction results. But at the same time, RCM 6.0 also led to a considerable reduction of sediment loads in a few downstream sub-basins. In addition, sediment loads were projected to vary between –70% and 110% under three remaining scenarios, RCM 2.6, 4.5, and 8.5. The decreasing pattern of sediment loads in individual sub-basins for RCM 2.6 was, in particular, quite similar to that of RCM 8.5 (Figs. 5a and d). Only, a small number of sub-basins appeared to show an increase in sediment loads under these two scenarios, as opposed to those in RCM 6.0. However, the decrease in sediment loads throughout the sub-basins was more pronounced in RCM 4.5 than in other scenarios (Fig. 5b). All these results revealed that RCM projections resulted in a significant change of sediment loads at the sub-basin level, but the extent of these changes was largely dependent on the characteristics of individual sub-basins such as topography, land use, agricultural activities, etc. We believe that a detailed discussion on the properties of individual sub-basins is out of the scope of this study.

3.3.3. Impact on TP loads

Fig. 6 exhibits the change in TP loads at the sub-basin scale modulated by four RCM scenarios. Note that the range of the color bar goes from –80% and 190%. Similar to those observed in streamflow and sediment loads, the (percent) change in TP loads at individual sub-basins was high in RCM 6.0 (Fig. 6c). Specifically, TP loads rose more than 50% in most of the sub-basins. However, the influence of both RCM 2.6 and 8.5 on the mean annual TP loads appeared to be quite similar to each other (Figs. 6a and d). In both scenarios, the percent change in TP loads was projected to range from –40% to 60% throughout the sub-basins. Also, an inverse relationship was observed between TP loads and RCM 4.5, where percent change estimated for individual sub-basins generally fell below 0% (Fig. 6b). In accordance with simulation results for other output variables, these results demonstrated that TP loads increased or

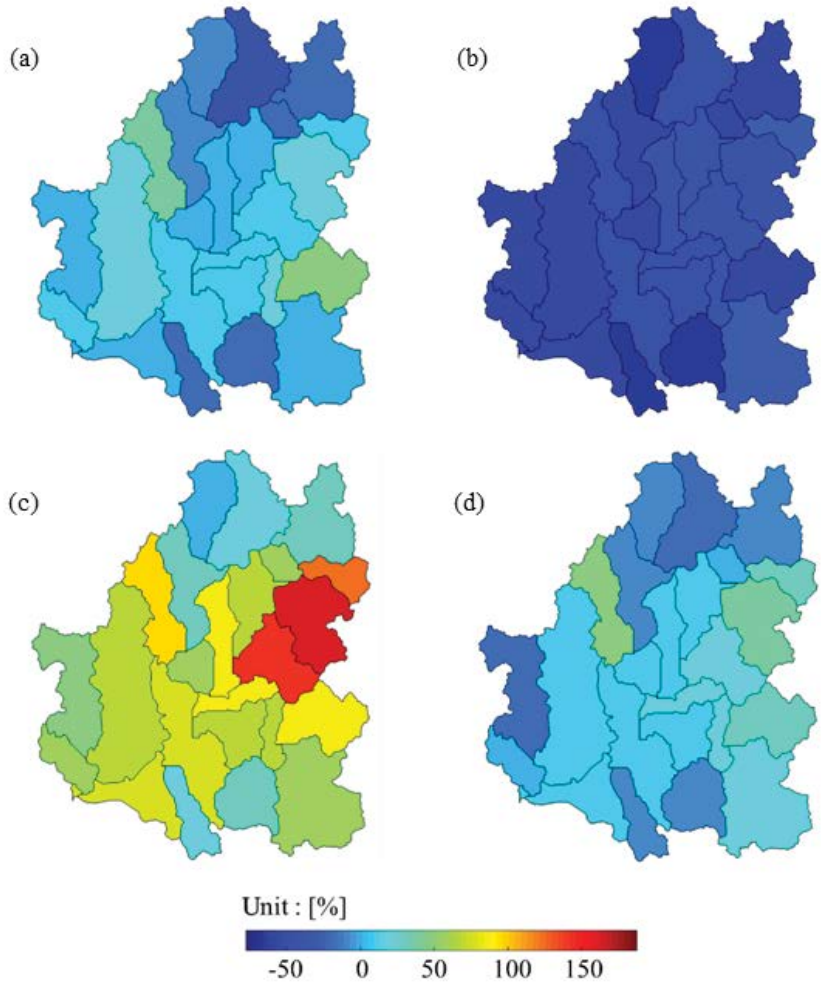

Fig. 6. Percent changes (%) in the predicted TP loads at the sub-basin scale under different future weather inputs in 2032: (a) RCM 2.6, (b) RCM 4.5, (c) RCM 6.0, and (d) RCM 8.5.

decreased heterogeneously across the sub-basins according to a combination of internal (i.e., the drainage characteristics) and external factors (i.e., the new weather inputs).

As a final step, we adopted the Kruskal–Wallis test, which allowed the one-way ANOVA test for non-normally distributed data, to examine the difference in three target variables among multiple groups, that is, the outputs among the sub-basins in each RCM projection and those at the entire watershed among all RCM scenarios (Table 2). From the table, it was found that there was no difference in sediment and TP loads among the sub-basins, whereas streamflow at individual sub-basins was largely affected by the new weather inputs, regardless of the radiative forcing levels. These results indicated that streamflow at the sub-basin level was more sensitive to the weather scenarios than sediment and TP loads which received indirect contributions through watershed processes controlling their fate and transport from weather events. However, streamflow as well as sediment load and TP loads at the watershed level were shown to vary significantly among RCM scenarios, implying that all three variables were susceptible to climate change impacts. These two results highlighted that there existed large discrepancies between watershed-wide and sub-basin management recommendations. For example, a watershed-scale management approach may be designed to minimize the effect of climate change on both water quantity and quality, whereas only water quantity aspect is taken into consideration at the sub-basin scale, according to different statistical test results. Therefore, it is essential to double-check simulation outputs at different spatial scales not only to fully account for the effects of new environmental conditions (such as RCM projections) on variables of interest, but also to implement proper actions in the watershed management planning process.

4. Conclusion

This study assessed water quantity and quality responses of the Yeongsan River Watershed in Korea with intensive agricultural production to changes in future local weather using SWAT. A series of simulations were performed using baseline (successfully validated in 2014) and new weather conditions (adopting four RCM scenarios,

Table 2
Results of the Kruskal–Wallis test on multiple groups of each variable predicted at the sub-basin and watershed levels under four future climate scenarios (i.e., RCM 2.6, 4.5, 6.0, and 8.5) in 2032

Variables	Units	Statistics	Sub-basin level				Watershed level
			RCM 2.6	RCM 4.5	RCM 6.0	RCM 8.5	All scenarios
Streamflow	m^3/s	χ^2	**1,412.02**[a]	**96.20**	**945.20**	**88.98**	**3,351.80**
Sediment loads	tons/y	χ^2	7.12	3.73	8.77	10.97	61.32
TP loads	kg/y	χ^2	2.94	21.84	4.00	13.88	42.83

[a]Note that p values less than 0.001 are indicated in bold. Also, the predicted outputs at the sub-basin level were averaged over the year 2032 for individual sub-basins, whereas the outputs at the watershed level are averaged over the year 2032, and then are averaged again for the entire watershed.

RCM 2.6, 4.5, 6.0, and 8.5, in 2032). The simulation outputs were then analyzed using a non-parametric Kruskal–Wallis test to identify a major contributor to variation of three target variables (i.e., streamflow as well as sediment and TP loads) at both watershed and sub-basin levels. The following conclusions were drawn in this study:

- Sensitivity analysis enabled proper correction of a series of key input parameters involved in computation of three target variables. Seven, four, and seven parameters adjusted for (daily) streamflow, (monthly) sediment loads, and (monthly) TP loads were within the reference ranges for the model, and achieved good performance with Nash–Sutcliffe efficiency values as low as 0.72 during calibration and validation.
- Providing additional future weather inputs to the model resulted in significant variation in three variables at the target watershed. The degree of variation in streamflow as well as sediment and TP loads varied depending on RCM scenarios. However, the statistical results found that no significant difference was observed in sediment and TP loads among 25 sub-basins according to each RCM scenario, whereas all three variables at the watershed scale differ substantially among the scenarios.

This discrepancy raises questions about the consistency of watershed management plans at different spatial scales and requests careful consideration on pollution mitigation strategies for area of concern.

Symbols

T — Temperature
W — Wind speed
H — Relative humidity
P — Precipitation
μ — Mean
σ — Standard deviation
CV — Coefficient of variation
d — Within daily interval

Sub-/superscripts

RCM,f — HadGEM3-RA simulated 2006–2100
RCM,h HadGEM3-RA simulated 1979–2005
obs Observed
M Within monthly interval
th Threshold level
* Final bias-corrected
*1,2 Bias-corrected in an intermediate step

Acknowledgments

This research was supported by the EDISON Program through the National Research Foundation of Korea (NRF) funded by the Ministry of Science and ICT (NRF-2017M3C1A6075011).

References

[1] Handbook for Developing Watershed Plans to Restore and Protect Our Waters, 2008.
[2] Watershed Management in Action—Lessons Learned from FAO Field Projects, 2017.
[3] E. Ahmadisharaf, R.A. Camacho, H.X. Zhang, M.M. Hantush, Y.M. Mohamoud, Calibration and validation of watershed models and advances in uncertainty analysis in TMDL studies, J. Hydrol. Eng., 24 (2019) 03119001, doi: 10.1061/(Asce)He.1943-5584.0001794.
[4] A. Ahani, S.S. Mousavi Nadoushani, A. Moridi, Simultaneous regionalization of gauged and ungauged watersheds using a missing data clustering method, J. Hydrol. Eng., 25 (2020) 04020015, doi: 10.1061/(ASCE)HE.1943-5584.0001916.
[5] M. Aghakhani, T. Nasrabadi, A. Vafaeinejad, Assessment of the effects of land use scenarios on watershed surface runoff using hydrological modelling, Appl. Ecol. Environ. Res., 16 (2018) 2369–2389.
[6] M. Ahmadi, R. Records, M. Arabi, Impact of climate change on diffuse pollutant fluxes at the watershed scale, Hydrol. Processes, 28 (2014) 1962–1972.
[7] C. Carvalho-Santos, A.T. Monteiro, J.C. Azevedo, J. Honrado, J.P. Nunes, Climate change impacts on water resources and reservoir management: uncertainty and adaptation for a mountain catchment in northeast Portugal, Water Resour. Manage., 31 (2017) 3355–3370.
[8] M. Babur, M.S. Babel, S. Shrestha, A. Kawasaki, N.K. Tripathi, Assessment of climate change impact on reservoir inflows using multi climate-models under RCPs the case of Mangla Dam in Pakistan, Water, 8 (2016) 389, doi: 10.3390/w8090389.
[9] C. Carvalho-Santos, J.P. Nunes, A.T. Monteiro, L. Hein, J.P. Honrado, Assessing the effects of land cover and future climate conditions on the provision of hydrological services in a medium-sized watershed of Portugal, Hydrol. Processes, 30 (2016) 720–738.
[10] V. Chaplot, Water and soil resources response to rising levels of atmospheric CO_2 concentration and to changes in precipitation and air temperature, J. Hydrol., 337 (2007) 159–171.

[11] L. Chen, G.Y. Wei, Z.Y. Shen, Incorporating water quality responses into the framework of best management practices optimization, J. Hydrol., 541 (2016) 1363–1374.
[12] L.C. Chiang, I. Chaubey, N.M. Hong, Y.P. Lin, T. Huang, Implementation of BMP strategies for adaptation to climate change and land use change in a pasture-dominated watershed, Int. J. Environ. Res Public Health, 9 (2012) 3654–3684.
[13] J.L. Qiu, Z.Y. Shen, X.S. Hou, H. Xie, G.Y. Leng, Evaluating the performance of conservation practices under climate change scenarios in the Miyun Reservoir Watershed, China, Ecol. Eng., 143 (2020) 105700, doi: 10.1016/j.ecoleng.2019.105700.
[14] C. Santhi, J.G. Arnold, J.R. Williams, L.M. Hauck, W.A. Dugas, Application of a watershed model to evaluate management effects on point and nonpoint source pollution, Trans. ASAE, 44 (2001) 1559–1570.
[15] Korea Ministry of Environment, 2020.
[16] South Korea Ministry of E. Water Resources Management Information System (WAMIS), 2003.
[17] The Importance of Watershed Management in Protecting Ontario's Drinking Water Supplies, 2001.
[18] Korea Meteorological Administration, 2020.
[19] J.H. Christensen, F. Boberg, O.B. Christensen, P. Lucas-Picher, On the need for bias correction of regional climate change projections of temperature and precipitation, Geophys. Res. Lett., 35 (2008) L20709, doi: 10.1029/2008GL035694.
[20] Climate Information Portal, 2017.
[21] G. Lenderink, A. Buishand, W. van Deursen, Estimates of future discharges of the river Rhine using two scenario methodologies: direct versus delta approach, Hydrol. Earth Syst. Sci., 11 (2007) 1143–1159.
[22] C. Teutschbein, J. Seibert, Bias correction of regional climate model simulations for hydrological climate-change impact studies: review and evaluation of different methods, J. Hydrol., 456 (2012) 12–29.
[23] K.L. White, I. Chaubey, Sensitivity analysis, calibration, and validations for a multisite and multivariable SWAT model, J. Am. Water Resour. Assoc., 41 (2005) 1077–1089.
[24] M.D. Mckay, R.J. Beckman, W.J. Conover, A comparison of three methods for selecting values of input variables in the analysis of output from a computer code, Technometrics, 42 (2000) 55–61.
[25] A. van Griensven, T. Meixner, S. Grunwald, T. Bishop, A. Diluzio, R. Srinivasan, A global sensitivity analysis tool for the parameters of multi-variable catchment models, J. Hydrol., 324 (2006) 10–23.
[26] M.D. Morris, Factorial sampling plans for preliminary computational experiments, Technometrics, 33 (1991) 161–174.
[27] K. Holvoet, A. van Griensven, P. Seuntjens, P.A. Vanrolleghem, Sensitivity analysis for hydrology and pesticide supply towards the river in SWAT, Phys. Chem. Earth, 30 (2005) 518–526.
[28] J.G. Arnold, J.R. Kiniry, R. Srinivasan, J.R. Williams, E.B. Haney, S.L. Neitsch, Soil and water Assessment Tool Input/Output File Documentation Version 2009, Texas Water Resources Technical Report No. 365, Texas, 2011.

Appendix A

The linear scaling method minimizes the difference between the average observation and simulation in a data period [21]. Precipitation was corrected with a ratio of the mean observations and simulations over the whole historical period (1979–2005). Other climatic data were corrected using the difference of the mean observations and simulations during the whole historical period (1979–2005). The monthly linear scaling of RCM outputs with monthly correction values should be consistent with the observed monthly mean values by definition. The RCM climate data are revised with the difference of monthly mean observations and simulations as follows:

$$T^*_{\mathrm{RCM},h}(d) = T_{\mathrm{RCM},h}(d) + \mu_m\left(T_{\mathrm{obs}}(d)\right) - \mu_m\left(T_{\mathrm{RCM},h}(d)\right) \quad (1)$$

$$T^*_{\mathrm{RCM},f}(d) = T_{\mathrm{RCM},f}(d) + \mu_m\left(T_{\mathrm{obs}}(d)\right) - \mu_m\left(T_{\mathrm{RCM},h}(d)\right) \quad (2)$$

$$H^*_{\mathrm{RCM},h}(d) = H_{\mathrm{RCM},h}(d) + \mu_m\left(H_{\mathrm{obs}}(d)\right) - \mu_m\left(H_{\mathrm{RCM},h}(d)\right) \quad (3)$$

$$H^*_{\mathrm{RCM},f}(d) = H_{\mathrm{RCM},f}(d) + \mu_m\left(H_{\mathrm{obs}}(d)\right) - \mu_m\left(H_{\mathrm{RCM},h}(d)\right) \quad (4)$$

$$W^*_{\mathrm{RCM},h}(d) = W_{\mathrm{RCM},h}(d) + \mu_m\left(W_{\mathrm{obs}}(d)\right) - \mu_m\left(W_{\mathrm{RCM},h}(d)\right) \quad (5)$$

$$W^*_{\mathrm{RCM},f}(d) = W_{\mathrm{RCM},f}(d) + \mu_m\left(W_{\mathrm{obs}}(d)\right) - \mu_m\left(W_{\mathrm{RCM},h}(d)\right) \quad (6)$$

A combination of local intensity scaling and power transformation scaling corrections for precipitation takes the following steps:

Firstly, a precipitation threshold (P_{th}) is specified to redefine precipitation under P_{th} to dry days with 0 mm of precipitation. The threshold of precipitation is set to 0.5 mm:

$$P^{*1}_{\mathrm{RCM},h}(d) = \begin{cases} 0, & \text{if } P_{\mathrm{RCM},h}(d) < P_{\mathrm{th}} \\ P_{\mathrm{RCM},f}(d), & \text{otherwise} \end{cases} \quad (7)$$

$$P^{*1}_{\mathrm{RCM},f}(d) = \begin{cases} 0, & \text{if } P_{\mathrm{RCM},f}(d) < P_{\mathrm{th}} \\ P_{\mathrm{RCM},f}(d), & \text{otherwise} \end{cases} \quad (8)$$

Finding b_m must satisfy:

$$CV_m\left(P_{\mathrm{obs}}(d)\right) - CV_m\left(\left(P^{*1}_{\mathrm{RCM},h}\right)^{b_m}(d)\right) = \frac{\sigma_m\left(P_{\mathrm{obs}}(d)\right)}{\mu_m\left(P_{\mathrm{obs}}(d)\right)} - \frac{\sigma_m\left(\left(P^{*1}_{\mathrm{RCM},h}\right)^{b_m}(d)\right)}{\mu_m\left(\left(P^{*1}_{\mathrm{RCM},h}\right)^{b_m}(d)\right)} = 0 \quad (9)$$

Then,

$$P^{*2}_{\mathrm{RCM},h}(d) = \left(P^{*1}_{\mathrm{RCM},h}\right)^{b_m}(d) \quad (10)$$

$$P^{*2}_{\mathrm{RCM},f}(d) = \left(P^{*1}_{\mathrm{RCM},f}\right)^{b_m}(d) \quad (11)$$

Intermediary precipitation is then corrected with a ratio of monthly mean intermediary precipitation and observation:

$$P^*_{\mathrm{RCM},h}(d) = P^{*2}_{\mathrm{RCM},h}(d) \cdot \left[\frac{\mu_m\left(P_{\mathrm{obs}}(d)\right)}{\mu_m\left(P^{*2}_{\mathrm{RCM},h}(d)\right)}\right] \quad (12)$$

$$P^*_{\mathrm{RCM},f}(d) = P^{*2}_{\mathrm{RCM},f}(d) \cdot \left[\frac{\mu_m\left(P_{\mathrm{obs}}(d)\right)}{\mu_m\left(P^{*2}_{\mathrm{RCM},h}(d)\right)}\right] \quad (13)$$